Earth and Planetary Science Letters 301 (2011) 256–264

Contents lists available at ScienceDirect

Earth and Planetary Science Letters

journal homepage: www.elsevier.com/locate/epsl

Decoupled warming and monsoon precipitation in East Asia over the last deglaciation

Francien Peterse [a,*], Maarten A. Prins [b], Christiaan J. Beets [b], Simon R. Troelstra [b], Hongbo Zheng [c], Zhaoyan Gu [d], Stefan Schouten [a], Jaap S. Sinninghe Damsté [a]

[a] NIOZ Royal Netherlands Institute for Sea Research, Department of Marine Organic Biogeochemistry, PO Box 59, 1790 AB Den Burg, Texel, The Netherlands
[b] VU University Amsterdam, Faculty of Earth and Life Sciences, Amsterdam, The Netherlands
[c] School of Earth Science and Engineering, Nanjing University, Nanjing 210093, China
[d] Institute of Geology and Geophysics, Chinese Academy of Sciences, Beijing 100029, China

ARTICLE INFO

Article history:
Received 9 June 2010
Received in revised form 11 October 2010
Accepted 7 November 2010
Available online 4 December 2010

Editor: P. DeMenocal

Keywords:
East Asian monsoon
air temperature
branched glycerol dialkyl glycerol tetraether (GDGT) membrane lipid
loess
paleoclimate
deglaciation

ABSTRACT

Our understanding of the continental climate development in East Asia is mainly based on loess–paleosol sequences and summer monsoon precipitation reconstructions based on oxygen isotopes ($\delta^{18}O$) of stalagmites from several Chinese caves. Based on these records, it is thought that East Asian Summer Monsoon (EASM) precipitation generally follows Northern Hemisphere (NH) summer insolation. However, not much is known about the magnitude and timing of deglacial warming on the East Asian continent. In this study we reconstruct continental air temperatures for central China covering the last 34,000 yr, based on the distribution of fossil branched tetraether membrane lipids of soil bacteria in a loess–paleosol sequence from the Mangshan loess plateau. The results indicate that air temperature varied in phase with NH summer insolation, and that the onset of deglacial warming at ~19 kyr BP is parallel in timing with other continental records from e.g. Antarctica, southern Africa and South-America. The air temperature increased from ~15 °C at the onset of the warming to a maximum of ~27 °C in the early Holocene (~12 kyr BP), in agreement with the temperature increase inferred from e.g. pollen and phytolith data, and permafrost limits in central China. Comparison of the tetraether membrane lipid-derived temperature record with loess–paleosol proxy records and stalagmite $\delta^{18}O$ records shows that the strengthening of EASM precipitation lagged that of deglacial warming by ca. 3 kyr. Moreover, intense soil formation in the loess deposits, caused by substantial increases in summer monsoon precipitation, only started around 12 kyr BP (ca. 7 kyr lag). Our results thus show that the intensification of EASM precipitation unambiguously lagged deglacial warming and NH summer insolation, and may contribute to a better understanding of the mechanisms controlling ice age terminations.

1. Introduction

Oxygen isotope ($\delta^{18}O$) records of stalagmites from several caves in China have yielded well dated, high-resolution records of the timing and amplitude of changes in East Asian Summer Monsoon (EASM) precipitation during the last four glacial–interglacial cycles (e.g. Cheng et al., 2009; Dykoski et al., 2005; Wang et al., 2001, 2008; Yuan et al., 2004). Generally, these records revealed that the EASM follows Northern Hemisphere (NH) insolation patterns. Similarly, various climate-proxy records derived from loess–paleosol sequences from the Chinese Loess Plateau have also documented changes in EASM precipitation (e.g. An, 2000; Heslop et al., 1999; Porter and An, 1995; Sun and Huang, 2006; Wu et al., 2002). The build-up of the loess plateau relates to changes in monsoon intensity, varying temperature and moisture conditions; loess is mainly deposited during cool and dry periods, as a result of an intensified winter monsoon, whereas soil formation takes place predominantly during the warmer and wetter periods with strengthened summer monsoon (Porter and An, 1995). The loess–paleosol records, as well as the stalagmite proxy records match the climatic changes in the North Atlantic that are recorded in Greenland ice-core records (Chen et al., 1997; Porter and An, 1995).

Although a large number of speleothem and loess records documenting EASM intensity have been generated, only little is known on the development of atmospheric temperature over the East Asian continent in relation to changes in monsoon precipitation intensity. Soil formation in loess sequences, caused by a substantial increase in summer monsoon precipitation, has been found to lag NH insolation (Heslop et al., 1999; Porter, 2001; Stevens et al., 2007). However, soil formation is not only stimulated by intensified summer monsoon precipitation, but by higher temperatures as well (Jenny, 1941).

* Corresponding author. Tel.: +31 222 369569; fax: +31 222 319674.
E-mail address: francien.peterse@nioz.nl (F. Peterse).

0012-821X
doi:10.1016/j.epsl.2010.11.010

To gain more insight into the exact timing and amplitude of eastern Asian continental temperature changes over the last glacial termination, we used the recently developed MBT/CBT (methylation of branched tetraethers/cyclisation of branched tetraethers) paleothermometer, based on branched glycerol dialkyl glycerol tetraethers (GDGTs) (Weijers et al., 2007b), in a loess–paleosol sequence of the Mangshan loess plateau (Fig. 1) to reconstruct a continuous temperature record for this area. Branched GDGTs are membrane lipids from bacteria that occur ubiquitously in soils and peat (Weijers et al., 2006, 2007b), and air temperatures can be reconstructed based on their distribution using the Methylation index of Branched Tetraethers (MBT) and the Cyclisation ratio of Branched Tetraethers (CBT) (Weijers et al., 2007b). The MBT/CBT proxy works well in geothermally heated soils (Peterse et al., 2009b) and branched GDGT distributions have been shown to reflect the adiabatic cooling of air along altitude gradients (Hren et al., 2010; Peterse et al., 2009a; Sinninghe Damsté et al., 2008). Also, when applied to marine surface sediments, branched GDGT-derived temperatures show good agreement with the annual mean air temperature of the adjacent river drainage basins (Rueda et al., 2009; Weijers et al., 2007a).

The paleosol–loess sequence from the Mangshan loess plateau investigated here mainly receives its sediment from the nearby Huang He floodplain (Yellow River), which has a relatively humid climate compared to the Central Loess Plateau. The available moisture enhances soil formation, and values of the branched and isoprenoid tetraether (BIT) index, that quantifies the content of soil-derived organic matter in a system, are therefore high for these soils (typically >0.8; Hopmans et al., 2004). This makes the sequence suitable for the application of the MBT/CBT proxy. This area is also ideal for a high-resolution reconstruction, as sedimentation rates are generally high (17 to 29 cm/kyr during the last 34 kyr; Prins et al., 2009; Zheng et al., 2007).

2. Material and methods

2.1. Sites and sampling

The Mangshan loess plateau lies 25 km west of Zhengzhou on the south bank of the Huang He (Fig. 1). The loess plateau is about 18 km in length (W–E) and 5 km in width (N–S), with its highest point reaching approximately 150 m above the Huang He floodplain. The Mangshan plateau receives ~645 mm precipitation per year, about 70% of which falls during the summer monsoon season (May–September). The air temperature is ~2 °C during the winter (December–February) and varies between 20 °C (May) and 27 °C (July) during the summer monsoon season. The mean annual air temperature is 15 °C (WMO, 2007). For this study, the upper part of the loess-pedogenic complex, covering the S0 (Holocene paleosol), L1 (last glacial loess deposit), and S1 (last interglacial paleosol) layers, has been sampled at two locations. The northern loess section, MS2006 (34°57.5′ N, 113°22.2′ E; Fig. 1C), is exposed on the northern slope of the Mangshan plateau, where the Huang He river and local gullies have cut through the loess, forming a valley with steep cliffs. The section is ~59 m thick and was continuously sampled in 36 partly-overlapping, freshly-dug, vertical trenches at a 5-cm resolution (Prins et al., 2009). At a southern location, two sections have been sampled, MS2008W (34°56.4′ N, 113°22.2′ E) and MS2008E (34°56.1′ N, 113°22.4′ E; Fig. 1C). Sections MS2008W and MS2008E are ~34 and ~14 m thick, respectively, and were sampled in total in 26

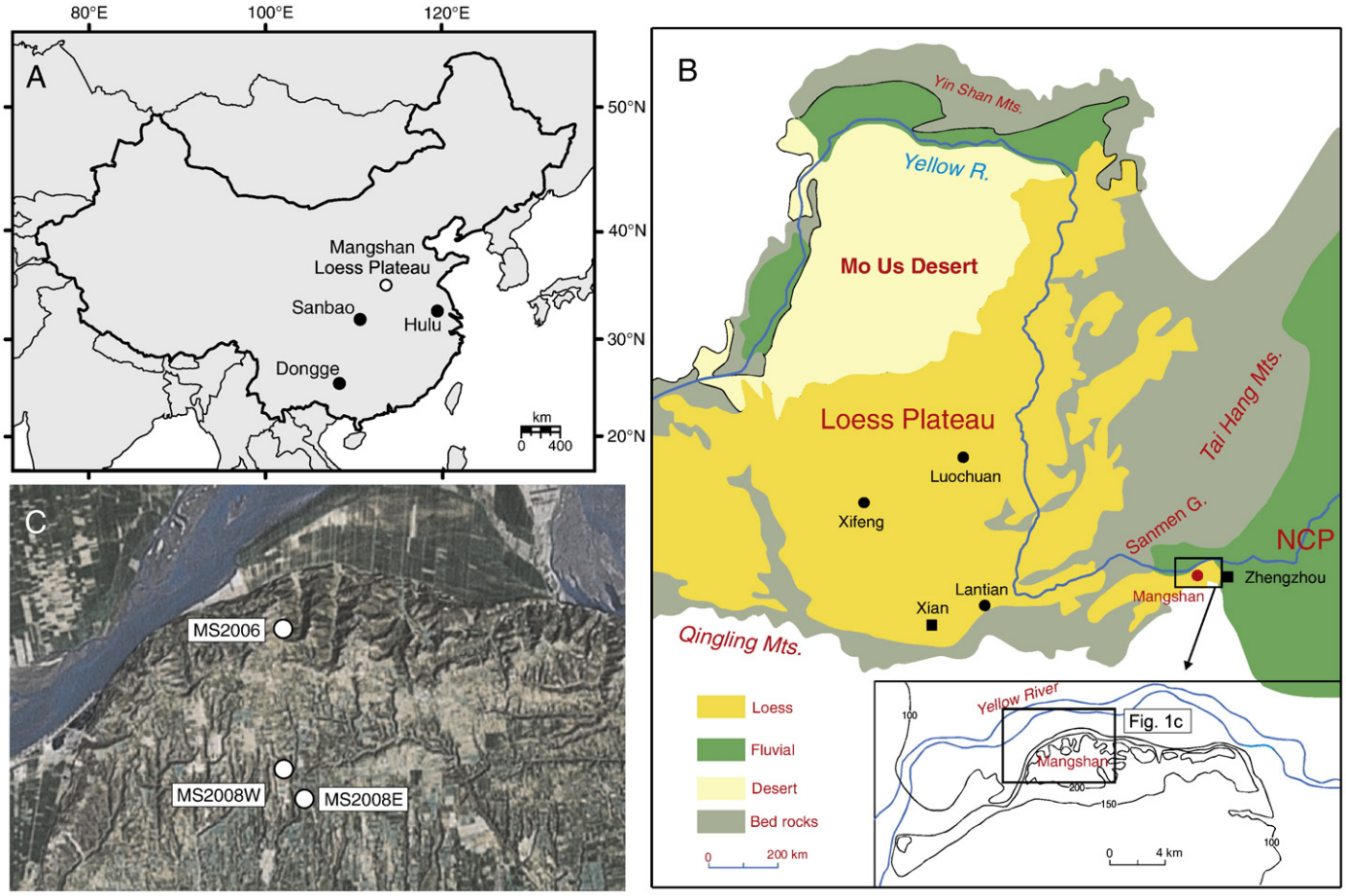

Fig. 1. Overview maps showing (A) China with the locations of the Mangshan Loess Plateau (white dot) and the Hulu, Sanbao, and Dongge caves (black dots), (B) the Chinese Loess Plateau, the Mo Us Desert and the North China Plain (NCP), and (C) the studied Mangshan loess sections. A blow up of the insert in (B) is shown in (C), and modified from Prins et al. (2009).

partly-overlapping vertical trenches at a 10-cm resolution. From field observations it is clear that the top part of the MS2008W section (0 to 45 cm) is disturbed by ploughing, as also evidenced by grain size data.

2.2. Magnetic susceptibility, organic matter and carbonate analysis

Samples were oven dried at 50 °C, lightly ground and aliquots of ~8 g were analyzed using a Bartington MS2 magnetic susceptibility meter at the School of Ocean and Earth Sciences, Tongji University. The organic matter and carbonate content of the samples were analyzed using a Leco TGA 601 at the VU University Amsterdam. Aliquots of ~2 g of the samples prepared for magnetic susceptibility analysis were used for thermo-gravimetric analysis (TGA).

2.3. Grain size analysis

Prior to the grain size measurement the samples were prepared according to the methods described by Konert and Vandenberghe (1997). Briefly, about 1–2 g of bulk sediment was pre-treated with solutions of 30% H_2O_2 and 1 N HCl in deinonized water to remove organic matter and carbonates, respectively. In case of a violent reaction, additional aliquots of H_2O_2 and/or HCl solution were added to ensure complete removal of organic matter and/or carbonates. Consequently, the results reflect the grain size distribution of the siliciclastic loess fraction. All measurements were performed on a Fritsch Analysette 22 laser particle sizer at the VU University Amsterdam. The variation in mean grain size for this particular instrument has been shown to be <0.5% (Jonkers et al., 2009). Grain size distributions were reported with 56 size classes between 0.15 and 2000 μm.

2.4. MBT/CBT analysis

Branched GDGTs were analyzed in the upper 5.9 m of section MS2008E and the upper 4.8 m of section MS2008W, using high performance liquid chromatography/atmospheric pressure chemical ionization-mass spectrometry (HPLC/APCI-MS) as described by Schouten et al. (2007), with minor modifications in the instrument settings, as mentioned below. The loess samples from the MS2008W sequence were freeze-dried. All loess samples from MS2008W and MS2008E were then homogenized with a mortar and pestle, and extracted (3×5 min) with a dichloromethane (DCM):methanol (9:1, v/v) mixture using an accelerated solvent extractor (ASE 200, Dionex) at 100 °C and 7.6×10^6 Pa. The total extracts were dried using a rotary evaporator under near vacuum, then dissolved in DCM and passed over a $NaSO_4$ column to remove any remaining water. Known amounts of an internal C_{46} GDGT standard were added according to Huguet et al. (2006). Separation of the extracts in apolar and polar fractions was done by passing them over an activated Al_2O_3 column using hexane:DCM (9:1, v/v) and DCM:MeOH (1:1, v/v), respectively. The polar fraction (containing the branched GDGTs and the internal standard) was dried under N_2, ultrasonically dissolved in hexane: isopropanol (99:1, v/v) and filtered over a 0.45 μm PTFE filter. The polar fractions were concentrated to about 3 mg/ml prior to analysis by HPLC/APCI-MS on an Agilent 1100 series LC/MSD SL. Separation of the branched GDGTs was achieved on an Alltech Prevail Cyano column (150 mm×2.1 mm; 3 μm). The compounds were eluted isocratically with 90% A and 10% B for 5 min (flow rate 0.2 ml/min), and then with a linear gradient to 16% B for 34 min, where A = hexane and B = hexane:isopropanol (9:1, v/v). The injection volume was 10 μl for each sample. Selective ion monitoring of the $[M+H]^+$ of the different GDGTs was used to detect and quantify them. Absolute quantification was achieved by calculating the area of the corresponding peaks in the chromatograms, comparing them with the peak area of the internal standard, and correcting them for the different response factors (cf. Huguet et al., 2006).

Air temperatures were calculated based on the MBT and CBT indices and the following transfer function as defined by Weijers et al. (2007b):

$$\mathrm{MBT} = 0.122 + 0.187 \times \mathrm{CBT} + 0.020 \times \mathrm{MAT} \left(r^2 = 0.77\right). \quad (1)$$

The average analytical reproducibility of the MBT and CBT indices, based on duplicate injections of a selected set of loess samples on the HPLC/APCI-MS, is 0.003 for the MBT index and 0.004 for the CBT index, resulting in an analytical error in temperature estimates of ca. 0.2 °C. The error introduced due to scatter in the calibration of Eq. (1) is much larger, ca. 5 °C (Weijers et al., 2007c), however, this uncertainty can be considered mainly systematic, and is caused by the global spread of the soils in the calibration set and the accompanying variation in environmental parameters. When the proxy is applied on a relatively small scale, like here on the Mangshan plateau, this systematic error is likely to be much smaller. However, an exact estimate of the error is difficult to constrain, given that a local calibration of the MBT/CBT proxy is not available. Nevertheless, absolute temperature estimates should be interpreted with caution.

3. Results and discussion

3.1. Age model

The age model of the Mangshan loess–paleosol sequences is based on the correlation of loess proxy records, i.e. magnetic susceptibility, carbonate content and grain size characteristics, with the U–^{230}Th dated oxygen isotope records from Dongge, Sanbao and Hulu caves in central China (Fig. 1A). The EASM $\delta^{18}O$ record is dominated by 23,000-year-long cycles that are synchronous (within dating errors) with summer insolation at 65°N (Berger, 1978), and the cycles are punctuated by millennial-scale strong summer monsoon events (Chinese interstadials; Cheng et al., 2006) and weak summer monsoon events (correlative with North Atlantic cold events, i.e. the Heinrich events; Wang et al., 2001). The ages of these events are exceptionally well constrained and may thus, as suggested by Wang et al. (2008), serve as benchmarks for correlating and calibrating climate records. The assumed match between the East Asian monsoon proxy records from the Mangshan loess–paleosol sequences and the Chinese speleothem records is independently supported by radiocarbon dating of fossil carbonate shells of land snails from a loess sequence close to site MS2006 for the time interval ~15–41 kyr BP (Fig. 2; Gu et al., 2009).

To match the proxy records of the Mangshan loess–paleosol sequence with the EASM $\delta^{18}O$ record, the carbonate and magnetic susceptibility records are used as tracers of soil development during humid interstadial and interglacial periods (cf. Maher and Thompson, 1992; Fig. 2). Consequently, carbonate minima and magnetic susceptibility maxima are correlated in time with the Chinese interstadials (speleothem $\delta^{18}O$ minima). The grain size profile is a tracer of eolian dust input, where clay content minima reflect periods of enhanced dust input and intensified winter monsoon, and is assumed to covary with the Chinese stadials (speleothem $\delta^{18}O$ maxima). Hence, matching of the loess proxy records of section MS2006 with the Sanbao/Hulu speleothem $\delta^{18}O$ record results in the age model shown in Fig. 2. The age models of sections MS2008W and MS2008E, that correlate very well to section MS2006 (Supplementary Figure 1), have been constructed in a similar way.

3.2. Continental air temperature record

The upper 5.9 m of loess–paleosol sequence MS2008E (Fig. 1C) corresponds to the last 34 kyr according to our age model. Branched GDGTs were detected throughout the whole loess–paleosol profile. Their concentrations vary between 1 and 13 ng GDGTs/g dry weight

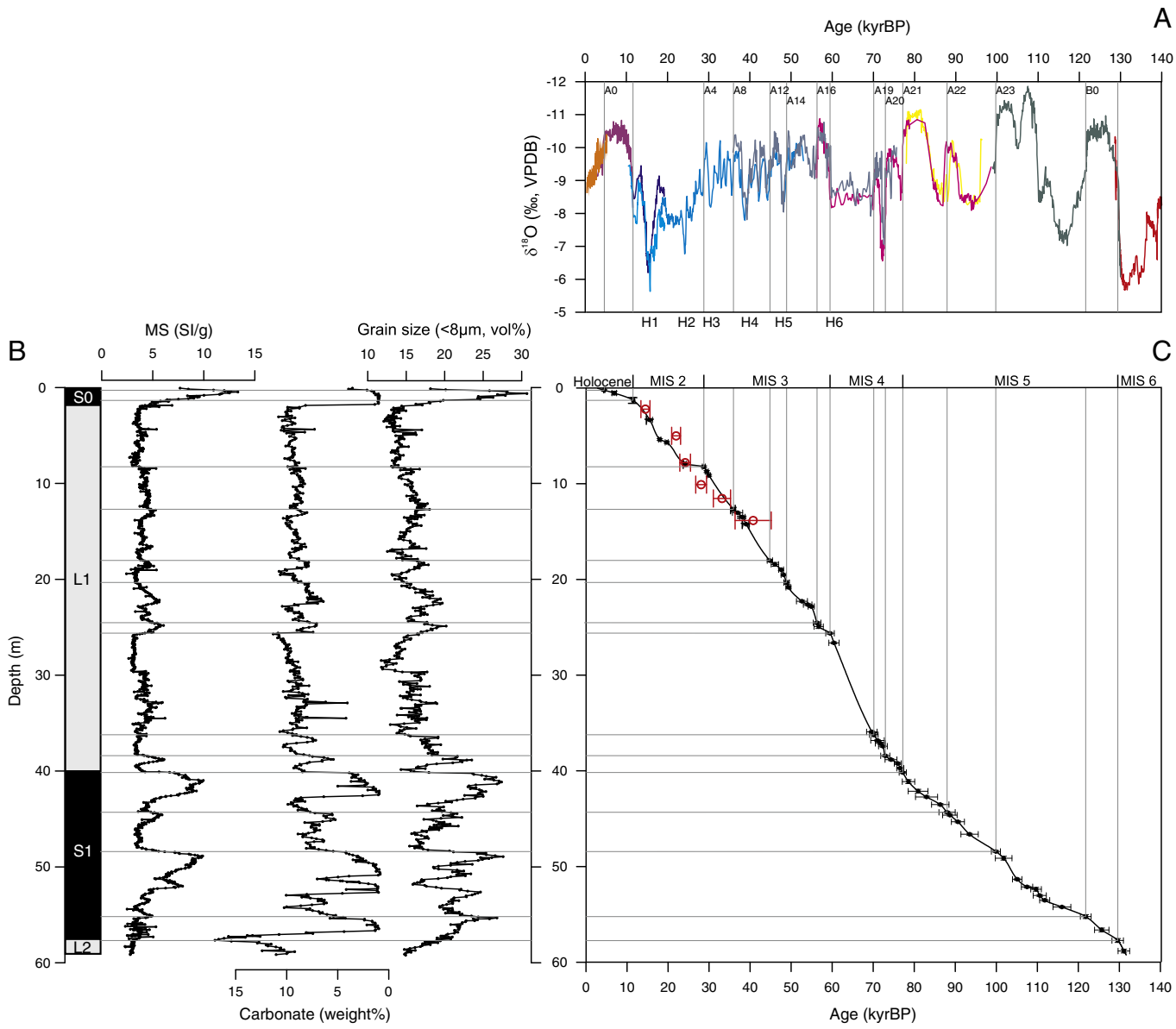

Fig. 2. Age model of the Mangshan loess record MS2006 based on correlation with the U–Th-dated Sanbao/Hulu speleothem $\delta^{18}O$ record of Wang et al., 2008 over the past ~131 kyr BP. (A) Time versus $\delta^{18}O$ in the Sanbao (red, stalagmite SB11; green, SB23; yellow, SB25-1; pink, SB22; dark blue, SB3; purple, SB10 and orange, SB26) and Hulu cave (three different hues of lighter blue, PD, D and L) records (Wang et al., 2008). For comparison, the Hulu $\delta^{18}O$ record is plotted 1.6‰ more negative to account for the higher $\delta^{18}O$ values in the Hulu record compared to the Sanbao record (cf. Wang et al., 2008). Marine-isotope stages (Holocene/MIS1–MIS6), Heinrich events (H1–H6; Wang et al., 2001) and Chinese interstadials (cf. Cheng et al., 2006) are indicated. (B) Magnetic susceptibility, carbonate content (weight %) and grain size (expressed as clay content) compared to paleosol (S0 and S1) and loess (L1 and L2) stratigraphy in sections MS2006 (Prins et al., 2009). (C) Age–depth profile for loess record MS2006. Grey lines indicate the location of the 'age-control points' used to tie the loess to the speleothem record. Red open circles indicate the radiocarbon dates of land snails (Gu et al., 2009; Table 3).

loess (Table 1), and are higher in the paleosol layer than in the loess layer. Although atmospheric dust from the loess plateau has not been analyzed, branched GDGTs were below detection limit in a dust sample from near the West coast of Central Africa, suggesting that these components are unlikely to be transported through the atmosphere in large amounts (Hopmans et al., 2004). Thus, the branched GDGTs are likely produced in situ in the loess–paleosol sequence, and the MBT/CBT record, therefore, reflects local conditions of the Mangshan plateau area.

Calculation of the MBT and CBT indices and application of Eq. (1) for the whole sequence, resulted in a continuous air temperature record for the period covered by the MS2008E sequence (Fig. 3B; Table 1). The MBT/CBT-derived temperature for the upper layer of MS2008E compares well with the average present-day air temperature (~24 °C) of the summer season (May–September) on the Mangshan plateau area (Fig. 3B), indicating that our record is most likely representing mean summer air temperatures. Although it is still unknown what group of bacteria is responsible for the production of branched GDGTs, and what their season of optimum growth is, microorganisms in general require moisture to live and grow. Since the Mangshan plateau receives over 70% of the annual amount of precipitation during the summer season (WMO, 2007), it is likely that this season is most suitable for bacterial productivity and thus the production of the branched GDGTs.

The MBT/CBT record reveals that summer air temperatures in the Mangshan plateau area were on average ~17 °C during the last glacial period, with a minimum of about 14 °C during the Last Glacial Maximum (LGM; ~21 kyr BP). The onset of deglacial warming around 19 kyr BP shown by our record matches with Antarctic warming (Fig. 4E), and is

Table 1
Depth, age, grain size (clay content), magnetic susceptibility (MS), organic matter (OM), branched GDGT abundance, and MBT/CBT-derived temperatures of paleosol–loess sequence MS2008E.

Depth (cm)	Age (kyr BP)	<8 μm (%)	MS	OM (%)	Branched GDGTs (ng/g dwt loess)	MBT/CBT-derived MAT (°C)
3.75	0.4	13.3	7.4	0.9	1.5	23.4
3.85	1.3	12.5	7.6	0.8	1.6	22.9
3.95	2.2	13.3	7.7	0.9	1.8	22.7
4.05	3.2	14.0	8.4	0.9	3.1	23.7
4.15	4.2	19.7	10.3	1.3	6.3	26.0
4.25	5.7	24.0	12.3	1.5	13.1	26.3
4.35	8.7	25.9	11.9	1.6	11.9	26.5
4.45	9.7	23.5	9.2	1.3	10.8	25.8
4.55	10.4	22.0	8.3	1.2	9.6	26.0
4.65	11.0	21.2	7.6	1.1	10.6	25.3
4.75	11.5	21.4	8.2	1.1	8.2	26.5
4.85	12.0	19.2	7.2	1.1	11.0	26.7
4.95	12.4	17.9	5.8	0.9	6.0	27.2
5.05	12.8	19.5	7.1	1.0	3.9	26.1
5.15	13.2	18.7	6.7	1.0	3.2	25.8
5.25	13.6	16.1	5.3	0.9	2.5	25.1
5.35	14.0	17.8	6.1	1.0	3.0	24.4
5.45	14.3	15.2	4.5	0.9	1.7	24.6
5.55	14.6	19.1	6.7	1.0	1.9	24.3
5.65	14.8	16.0	4.3	0.8	2.5	23.8
5.75	15.0	16.4	4.7	0.8	2.8	24.5
5.85	15.1	14.9	3.7	0.7	1.2	22.3
5.95	15.2	14.2	4.8	0.8	1.8	20.8
6.05	15.3	14.9	4.2	0.8	2.7	21.6
6.15	15.3	15.3	4.2	0.8	2.5	22.6
6.25	15.4	13.7	4.0	0.8	2.0	21.5
6.35	15.5	12.9	3.6	0.8	2.0	20.9
6.45	15.5	13.5	3.8	0.8	2.0	21.1
6.55	15.7	12.5	3.9	0.8	2.1	19.4
6.65	15.8	11.8	4.2	0.7	2.1	20.4
6.75	16.0	12.8	3.9	0.7	1.6	20.0
6.85	16.3	13.8	4.1	0.7	1.6	19.1
6.95	16.7	13.7	4.0	0.7	1.7	18.7
7.05	17.2	14.1	4.1	0.7	1.7	19.3
7.15	17.6	13.8	4.3	0.7	3.1	15.3
7.25	18.0	14.4	4.3	0.8	2.6	19.5
7.35	18.3	14.1	4.6	0.7	2.7	17.5
7.45	18.5	14.0	4.7	0.8	4.0	14.7
7.55	18.8	13.2	4.5	0.8	2.4	15.3
7.65	19.1	13.6	4.3	0.8	2.0	15.6
7.75	19.4	13.3	4.2	0.7	1.7	14.9
7.85	19.7	13.1	3.9	0.7	1.3	17.3
7.95	20.1	13.4	3.9	0.7	1.4	15.9
8.05	20.5	13.5	4.1	0.7	2.5	15.1
8.15	20.9	13.3	4.2	0.7	2.4	15.0
8.25	21.3	12.9	4.6	0.7	2.0	13.5
8.35	21.8	12.9	4.2	0.7	1.9	16.3
8.45	22.4	13.5	4.5	0.7	1.0	16.8
8.55	22.9	13.2	4.2	0.8	0.8	15.6
8.65	23.5	13.0	4.1	0.6	1.6	16.2
8.75	24.2	13.1	4.2	0.6	0.9	17.1
8.85	25.0	13.7	4.1	0.7	2.1	15.3
8.95	25.9	14.1	4.2	0.7	1.8	18.1
9.05	27.0	14.6	4.0	0.7	1.5	18.1
9.15	28.2	15.8	4.6	0.7	2.4	19.0
9.25	29.4	15.4	4.7	0.8	2.7	17.9
9.35	30.5	15.7	4.6	0.8	1.8	18.9
9.45	31.5	15.9	–[a]	0.8	2.2	18.1
9.55	32.6	16.5	4.8	0.8	2.3	18.4
9.65	33.6	16.2	5.0	0.8	2.9	16.9

[a] Not determined.

similar in timing with mid-latitude glacier retreat at the end of the LGM, as indicated by ^{10}Be exposure dates of boulders in moraines on both northern and southern hemispheres (Schaeffer et al., 2006). Also, TEX_{86}-inferred lake surface temperature reconstructions for lakes Malawi and Tanganyika suggest a similar timing of deglacial warming in southern Africa (Powers et al., 2005; Tierney et al., 2008), while atmospheric warming in tropical central Africa, reconstructed with the MBT/CBT proxy, may have started slightly later (Weijers et al., 2007a; Fig. 4D).

The reconstructed summer air temperatures in the Mangshan plateau area show an increase from ~15 °C at the onset of deglacial warming to ~27 °C at the beginning of the Holocene (~12 kyr BP), with an average rate of almost 2 °C/kyr. The difference between the present-day mean summer temperature (~24 °C) and the reconstructed air temperature during the LGM (~17 °C) is in agreement with other studies from this region: estimates based on pollen studies and permafrost limits in central China suggest 7–10 °C cooler air temperatures during the LGM (Zhou et al., 1998), whereas other pollen assemblage (Sun et al., 1997) or phytolith-based (Lu et al., 2007) temperature reconstructions suggest that the air temperature at that time was 4.5–9 °C cooler than present.

Maximum air temperatures on the Mangshan plateau occurred at the loess (L1) to paleosol (S0) transition that marks the beginning of the Holocene (Fig. 3). During the Holocene climatic optimum, which was around 6–7 kyr BP for this part of China (An, 2000), air temperatures were ca. 3 °C higher compared to present. This temperature difference is slightly larger than the ca. 1 °C suggested by the modelling study of Tao et al. (2010), although the proxy data that they use to compare their model with, suggest 2–3 °C higher temperatures (Tao et al., 2010 and reference therein), which is again in agreement with the MBT/CBT-derived record. Similar temperature estimates are reported based on pollen records (Zhou et al., 1998; 1–6 °C warmer than present, depending on the geographical location), and phytoliths (Lu et al., 2007; 1–2 °C warmer than present).

Evidence for the robustness of our temperature record, next to the generally good fit with previously published temperature estimates and trends, is provided by the analysis of the upper 4.8 m of the nearby loess–paleosol sequence MS2008W (Fig. 1C). According to our age model, this sequence covers the last 16 kyr. Since the top 45 cm is disturbed because of ploughing, the upper 3 samples are excluded from the discussion. The branched GDGT concentrations varied between 2 and 27 ng/g dwt loess (Table 2), showing the same variations with depth as seen in the MS2008E sequence. Comparison of the two resulting temperature records shows a similar timing and magnitude of deglacial warming, as well as absolute temperature estimates (Fig. 4B,C; Table 2).

3.2. Comparison with NH summer insolation, loess–paleosol proxy records and stalagmite $\delta^{18}O$ records

Our MBT/CBT record shows that summer air temperatures at the Mangshan plateau area have developed in phase with NH summer insolation throughout the whole record (Fig. 3), and that the onset of atmospheric warming is parallel in timing with that on Antarctica. Interestingly, the clay fraction, magnetic susceptibility, and organic carbon content that were measured for the MS2008E sequence, lag the onset of atmospheric warming, and start to only slowly increase from ~16 kyr BP onwards (Monsoon Intensification 1, Fig. 3; Table 1). This implies that during the first period of significant warming, the climate at the Mangshan plateau was still relatively dry, and limited soil formation was taking place, like previously suggested by Wu et al. (2002) based on mollusc studies. Pedogenic processes intensified at the start of the Holocene (~12 kyr BP), resulting in the formation of the S0 paleosol. This signifies that only then summer monsoon precipitation intensified to such an extent that conditions became substantially wetter (Monsoon Intensification 2, Fig 3), as is also shown in other Chinese loess records (Stevens et al., 2007). Similar lags have been reported for Africa, where deglacial warming after the LGM seems to coincide with the temperature increase in Antarctica, but where the onset of increased precipitation, in contrast, matches with northern hemisphere climatic changes (Gasse, 2000; Tierney et al., 2008).

The considerable continental warming during the last glacial termination (up to 13 °C), may potentially have had an imprint on the $\delta^{18}O$ values recorded by the Chinese cave stalagmites, as this signal is

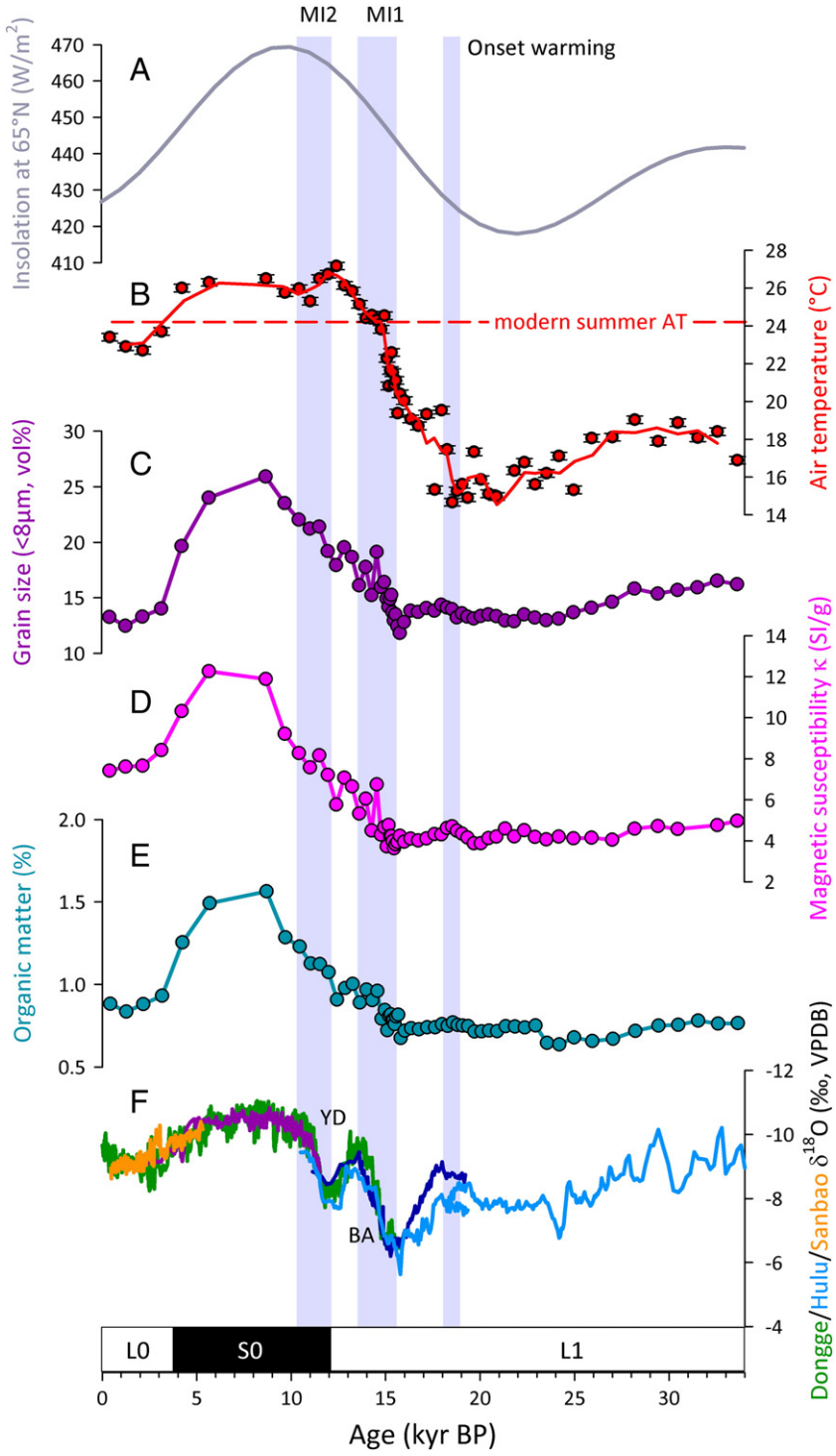

Fig. 3. Air temperature changes over the past 34 kyr for the Mangshan loess plateau area compared with Northern Hemisphere insolation and summer monsoon intensity. Records represent (A) Northern Hemisphere July insolation at 65°N (Berger, 1978), (B) 3 point moving average MBT/CBT-derived summer air temperatures for the MS2008E loess–paleosol sequence, with bars indicating the analytical error (C) grain size (expressed as clay content), (D) magnetic susceptibility, and (E) organic matter content for the MS2008E sequence, and (F) $\delta^{18}O$ records from Dongge (green; Dykoski et al., 2005), Sanbao (orange SB26, purple SB10, dark blue SB3; Wang et al., 2008), and Hulu Caves (light blue; Wang et al., 2001). For comparison, the Hulu and Dongge $\delta^{18}O$ records are plotted 1.6‰ more negative to account for the higher $\delta^{18}O$ values in the Hulu and Dongge records compared to the Sanbao record (cf. Wang et al., 2008). Grey bars indicate the onset of warming (~19 kyr BP) during the last glacial termination, and phases of increased summer monsoon precipitation at ~15 kyr BP (MI1) and at the start of the Holocene (~12 kyr BP; MI2) reflected by changes in the loess–paleosol proxy records. L0, S0 and L1 represent the Holocene loess, Holocene paleosol and last glacial loess layer, respectively, of the loess–paleosol sequence on the Mangshan Plateau.

not only influenced by precipitation, but also by temperature. Although care has to be taken in extrapolating our air temperatures to those of caves, the 5–6 °C increase in temperature from ~17 kyr BP onwards to the peak of the Bølling–Allerød interstadial at ~14 kyr BP in the composite speleothem record could potentially have shifted the corresponding part of the $\delta^{18}O$ records by ~1.3‰ towards more negative values (−0.24‰/°C, according to Friedman and O'Neil, 1977). This would imply that the intensification of EASM precipitation

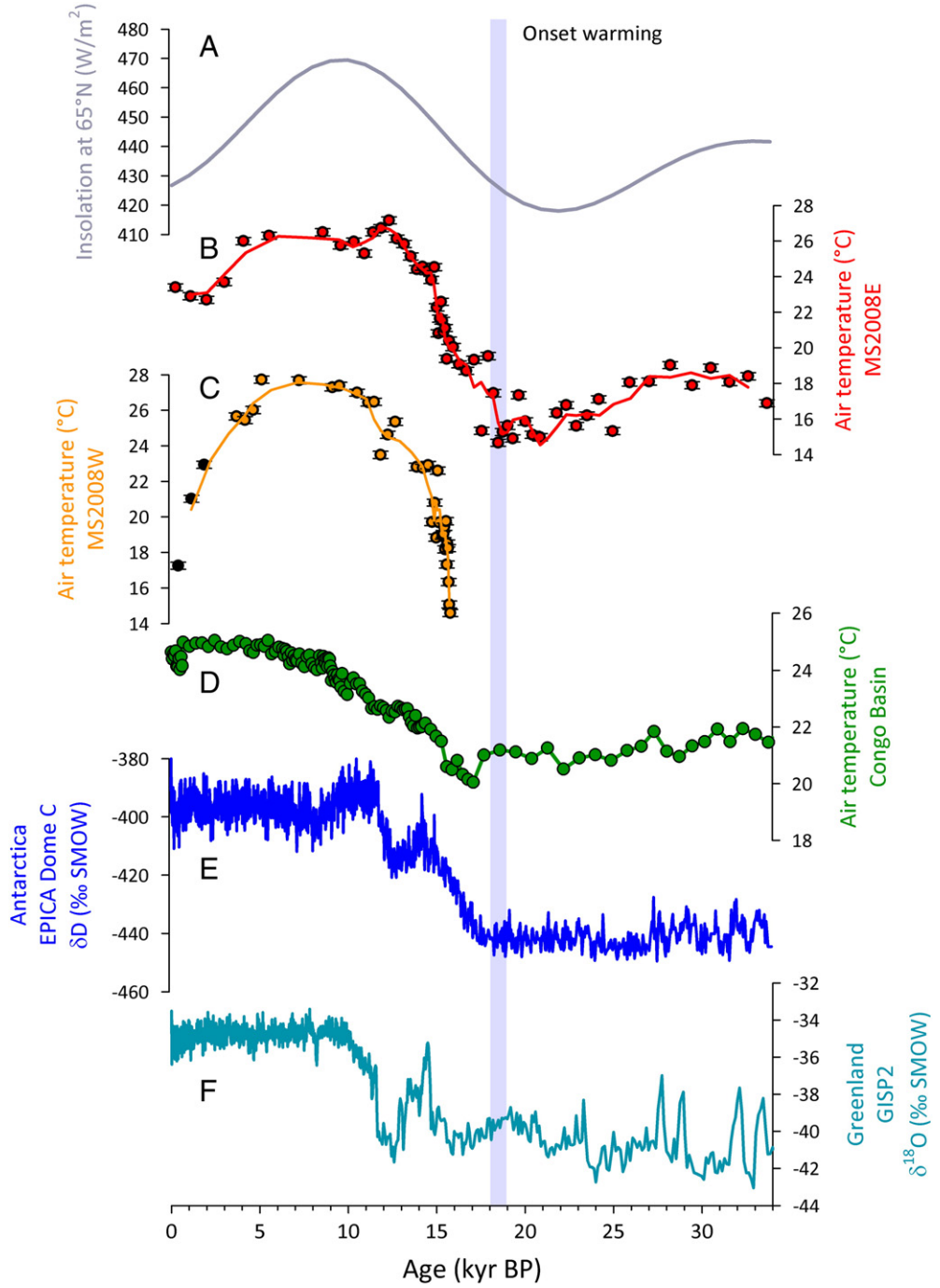

Fig. 4. Air temperature changes over the past 34 kyr for two loess–paleosol sequences from the Mangshan loess plateau area compared with Northern Hemisphere insolation, air temperatures from tropical Africa, and Antarctic and Arctic climate signals. Records represent (A) Northern Hemisphere July insolation at 65°N (Berger, 1978), (B) 3 point moving average MBT/CBT-derived air temperatures for the MS2008E and (C) the MS2008W loess–paleosol sequence, with bars indicating the analytical error. Disturbed samples from the MS2008W section are coloured black. (D) Air temperatures for the Congo Basin (Weijers et al., 2007a), (E) the EPICA Dome C δD record indicative of Antarctic air temperature changes (Jouzel et al., 2007) and (F) the Greenland Ice Sheet Project 2 (GISP2) $\delta^{18}O$ record indicative of Greenland air temperature fluctuations (Stuiver and Grootes, 2000).

during the initial stages of deglacial warming (Fig. 3; MI 1) would have been less intense than suggested by the $\delta^{18}O$ records. The substantial decrease in speleothem $\delta^{18}O$ values at the Younger Dryas to Holocene transition is only accompanied by minor air temperature changes, suggesting a large increase in EASM precipitation (Fig. 3; MI 2). This agrees well with the observed formation of the S0 paleosol, starting at ~12 kyr BP in our loess–paleosol record, as well as in other loess–paleosol records (Porter, 2001; Stevens et al., 2007). Thus, it seems that temperature has indeed affected the stalagmite $\delta^{18}O$ record, especially during times of rapid and large changes, i.e. during MI1.

Our records indicate that there is a considerable delay (up to ~7 kyr) in the intensification of EASM precipitation compared to continental warming and NH insolation. Several complex mechanisms have been put forward to explain the delayed response of EASM precipitation during glacial terminations. For example, latent heat export from the Southern Hemisphere Indian Ocean as well as glacial boundary conditions could have delayed the EASM onset (Clemens and Prell, 2007; Liu et al., 2006). It has also been hypothesized that the lag may have been caused by cold anomalies generated by disintegrating ice sheets and sea-ice formation in the North Atlantic region (Cheng et al., 2009). This would have generated a colder North

Table 2
Depth, age, branched GDGT abundance, and MBT/CBT-derived temperatures of paleosol–loess sequence MS2008W.

Depth (cm)	Age (kyr BP)	Branched GDGTs (ng/g dwt loess)	MBT/CBT-derived MAT (°C)
0.05[a]	0.4	13.3	17.2
0.15[a]	1.1	12.8	21.0
0.25[a]	1.9	9.9	22.9
0.55	3.7	14.2	25.7
0.65	4.2	13.7	25.4
0.75	4.6	15.4	26.0
0.85	5.1	21.9	27.7
1.15	7.2	26.8	27.7
1.45	9.1	17.5	27.3
1.55	9.5	9.1	27.4
1.85	10.5	7.0	27.0
2.05	11.2	7.6	26.4
2.15	11.5	6.9	26.5
2.25	11.9	3.5	23.5
2.35	12.3	3.0	24.6
2.45	12.7	4.0	25.3
2.75	13.9	3.0	22.8
2.85	14.3	2.6	22.8
2.95	14.6	5.8	22.9
3.05	14.8	2.2	19.7
3.15	15.0	3.1	20.8
3.25	15.0	2.7	18.8
3.35	15.1	3.3	22.6
3.45	15.2	2.7	19.7
3.75	15.4	2.1	18.9
3.85	15.5	3.0	19.0
3.95	15.5	5.2	19.4
4.05	15.6	3.8	18.2
4.15	15.6	1.6	19.7
4.25	15.6	3.0	17.3
4.35	15.7	2.4	18.5
4.45	15.7	3.6	18.2
4.55	15.7	2.1	16.3
4.65	15.8	3.8	15.1
4.75	15.8	1.8	14.6

[a] Disturbed sample.

Atlantic that, through atmospheric teleconnections, has led to a weakening of the East Asian summer monsoon intensity. The records from the Mangshan plateau indicate that over the last deglaciation, intensification of the East Asian summer monsoon was mainly influenced by northern hemisphere climatic changes, whereas atmospheric warming coincides with the temperature increase on Antarctica. Our results thus support the statistical evaluation of the controls of East Asian monsoon variability by Rohling et al. (2009), who suggested a southern hemisphere 'push' during glacial times when the monsoon is weak, i.e. between ~28 and ~16 kyr BP.

Regardless of the exact mechanisms, our data suggest that the factors controlling the onset of deglacial atmospheric warming and the intensification of EASM precipitation may have been different. Generation of MBT/CBT records in high sedimentation rate loess–paleosol sequences, such as those from the Mangshan Plateau, now offers the opportunity to constrain the timing and magnitude of continental temperature changes in eastern Asia. They can be used to obtain a more accurate assessment of hydrological and thermal changes in this climatologically important area.

Table 3
Calibrated radiocarbon dates of fossil aragonitic land snail shells in the MS2006 loess–paleosol sequence, inferred from Gu et al. (2009).

Depth (m)	Snail shells, calibrated age (kyr)	Error
2.175	14.6	1.1
4.975	22.1	1.1
7.775	24.3	1.3
10.075	28.2	1.3
11.525	33.3	2.1
13.825	40.9	4.4

Conclusions

The application of the MBT/CBT proxy on paleosol–loess sequences from the Mangshan loess plateau has resulted in a continuous, high-resolution air temperature record that provides an insight in the climate development of eastern Asia during the last 34,000 yr. The record shows that the onset of deglacial atmospheric warming is similar in timing with previous continental temperature records from e.g. Antarctica and Africa, and that air temperature varied in phase with Northern Hemisphere summer insolation. However, deglacial intensification of the East Asian Summer Monsoon, based on loess proxy records obtained from the same paleosol–loess sequence and $\delta^{18}O$ speleothem records, clearly lagged that of warming by >3 kyr. Intense soil formation (i.e. development of the Holocene paleosol S0), depending on both higher temperatures and available moisture, even lagged deglacial warming by ~7 kyr. Our data and new MBT/CBT-derived temperature records may give us the opportunity to better understand the driving forces of deglacial warming and the monsoon system in eastern Asia.

Supplementary materials related to this article can be found online at doi:10.1016/j.epsl.2010.11.010.

Acknowledgements

We would like to thank two anonymous reviewers and Dr. DeMenocal for constructive comments. We also like to thank Martin Konert, Patrick Bacon, Ilse Kamerling, Wouter Wester, Noortje Dijkstra, Daniel Rits, Noortje Vroomans, Wieske Wentink, Hugo Wester from VU University Amsterdam, Huang Xiangtong, Bin Zhou, Ke Wang, Jia Juntao from Tongji University, and Ellen Hopmans, Jort Ossebaar, Anchelique Mets, and Jaap van der Meer from Royal NIOZ for discussion and assistance with lab and fieldwork. MAP, CJB, SRT, HZ and ZG thank the KNAW for financial support (PSA-E-02, 06CDP041 and 08CDP021 projects). JSSD and SS received funding from the ERC project PACEMAKER. This is publication number DW-2010-1010 of the Darwin Center for Biogeosciences, which partially funded this project.

References

An, Z., 2000. The history and variability of the East Asian paleomonsoon climate. Quatern. Sci. Rev. 19, 171–187.
Berger, A.L., 1978. Long-term variations of caloric insolation resulting from the Earth's orbital elements. Quatern. Res. 9, 139–167.
Chen, F.H., Bloemendal, J., Wang, J.M., Oldfield, F., 1997. High-resolution multi-proxy climate records from Chinese loess: evidence for rapid climatic changes over the last 75 kyr. Palaeogeogr. Palaeocl. 130, 323–335.
Cheng, H., Edwards, L., Wang, Y., Kong, X., Ming, Y., Kelly, M.J., Wang, X., Gallup, C.D., Liu, W., 2006. A penultimate glacial monsoon record from Hulu Cave and two phase glacial terminations. Geology 34, 217–220.
Cheng, H., Edwards, R.L., Broecker, W.S., Denton, G.H., Kong, X., Wang, Y., Zhang, R., Wang, X., 2009. Ice age terminations. Science 326, 248–252.
Clemens, S.C., Prell, W.L., 2007. The timing of orbital-scale Indian monsoon changes. Quatern. Sci. Rev. 26, 275–278.
Dykoski, C.A., Edwards, R.L., Cheng, H., Yuan, D., Cai, Y., Zhang, M., Lin, Y., Qing, J., An, Z., Revenaugh, J., 2005. A high-resolution, absolute-dated Holocene and deglacial Asian monsoon record from Dongge Cave, China. Earth Planet. Sc. Lett. 233, 71–86.
Friedman, I., O'Neil, J.R., 1977. Data of geochemistry, I. In: Friedman, O'Neil, J.R. (Eds.), U.S. Geological Survey (USGS) Professional Paper 440-KK, KK1-12, USGS, Washington, DC.
Gasse, F., 2000. Hydrological changes in the African tropics since the Last Glacial Maximum. Quatern. Sci. Rev. 19, 189–211.
Gu, Z., Liu, Z., Xu, B., Wu, N., 2009. Stable carbon and oxygen isotopes in land snail carbonate shells from a last glacial loess sequence and their implications of environmental changes. Quatern. Sci. 29, 13–22 (in Chinese with English abstract).
Heslop, D., Shaw, J., Bloemendal, J., Chen, F., Wang, J., Parker, E., 1999. Sub-millennial scale variations in East Asian monsoon systems recorded by dust deposits from the north-western Chinese Loess Plateau. Phys. Chem. Earth 24, 785–792.
Hopmans, E.C., Weijers, J.W.H., Schefuß, E., Herfort, L., Sinninghe Damsté, J.S., Schouten, S., 2004. A novel proxy for terrestrial organic matter in sediments based on branched and isoprenoid tetraether lipids. Earth Planet. Sc. Lett. 224, 107–116.

Hren, M.T., Pagani, M., Erwin, D.M., Brandon, M., 2010. Biomarker reconstruction of the early Eocene paleotopography and paleoclimate of the northern Sierra Nevada. Geology 38, 7–10.
Huguet, C., Hopmans, E.C., Febo-Ayala, W., Thompson, D.H., Sinninghe Damsté, J.S., Schouten, S., 2006. An improved method to determine the absolute abundance of glycerol dibiphytanyl glycerol tetraether lipids. Org. Geochem. 37, 1036–1041.
Jenny, H., 1941. Factors of Soil Formation. McGraw-Hill, New York.
Jonkers, L., Prins, M.A., Brummer, G.-J., Konert, M., Lougheed, B.C., 2009. Experimental insights into laser diffraction particle sizing of fine-grained sediments for use in palaeoceanography. Sedimentology 56, 2192–2206.
Jouzel, J., Masson-Delmotte, V., Cattani, O., Dreyfus, G., Falourd, S., Hoffmann, G., Minster, B., Nouet, J., Barnola, J.M., Chappellaz, J., Fischer, H., Gallet, J.C., Johnsen, S., Leuenberger, M., Loulergue, L., Luethi, D., Oerter, H., Parrenin, F., Raisbeck, G., Raynaud, D., Schilt, A., Schwander, J., Selmo, E., Souchez, R., Spahni, R., Stauffer, B., Steffensen, J.P., Stenni, B., Stocker, T.F., Tison, J.L., Werner, M., Wolff, E.W., 2007. Orbital and millennial Antarctic climate variability over the past 800,000 years. Science 317, 793–796.
Konert, M., Vandenberghe, J., 1997. Comparison of laser grain size analysis with pipette and sieve analysis: a solution for the underestimation of the clay fraction. Sedimentology 44, 523–535.
Liu, X., Liu, Z., Kutzbach, J.E., Clemens, S.C., Prell, W.L., 2006. Hemispheric insolation forcing of the Indian Ocean and Asian Monsoon: local versus remote impacts. J. Climate 19, 6195–6208.
Lu, H.-Y., Wu, N.-Q., Liu, K.-B., Jiang, H., Liu, T.-S., 2007. Phytoliths as quantitative indicators for the reconstruction of past environmental conditions in China II: palaeoenvironmental reconstruction in the Loess Plateau. Quatern. Sci. Rev. 26, 759–772.
Maher, B.A., Thompson, R., 1992. Paleoclimatic significance of the mineral magnetic record of the Chinese loess and paleosols. Quatern. Res. 37, 155–170.
Peterse, F., van der Meer, M.T.J., Schouten, S., Jia, G., Ossebaar, J., Blokker, J., Sinninghe Damsté, J.S., 2009a. Assessment of soil *n*-alkane δD and branched tetraether membrane lipid distributions as tools for paleoelevation reconstruction. Biogeoscience 6, 2799–2807.
Peterse, F., Schouten, S., van der Meer, J., van der Meer, M.T.J., Sinninghe Damsté, J.S., 2009b. Distribution of branched tetraether lipids in geothermally heated soils: implications for the MBT/CBT temperature proxy. Org. Geochem. 40, 201–205.
Porter, S.C., 2001. Chinese loess record of monsoon climate during the last glacial–interglacial cycle. Earth Sci. Rev. 54, 115–128.
Porter, S.C., An, Z., 1995. Correlation between climate events in the North Atlantic and China during the last glaciations. Nature 375, 305–308.
Powers, L.A., Johnson, T.C., Werne, J.P., Castañeda, I.C., Hopmans, E.C., Sinninghe Damsté, J.S., Schouten, S., 2005. Large temperature variability in the southern African tropics since the Last Glacial Maximum. Geophys. Res. Lett. 32, L08706.
Prins, M.A., Zheng, H., Beets, K., Troelstra, S., Bacon, P., Kamerling, I., Wester, W., Konert, M., Huang, X., Ke, W., Vandenberghe, J., 2009. Dust supply from river floodplains: the case of the lower Huang He (Yellow River) recorded in a loess–palaeosol sequence from the Mangshan Plateau. J. Quatern. Sci. 24, 75–84.
Rohling, E.J., Liu, Q.S., Roberts, A.P., Stanford, J.D., Rasmussen, S.O., Langen, P.L., Siddall, M., 2009. Controls on the East Asian monsoon during the last glacial cycle, based on comparison between Hulu Cave and polar ice-core records. Quatern. Sci. Rev. 28, 3291–3302.
Rueda, G., Rosell-Melé, A., Escala, M., Gyllencreutz, R., Backman, J., 2009. Comparison of instrumental and GDGT-based estimates of sea surface and air temperatures from the Skagerrak. Org. Geochem. 40, 287–291.
Schaeffer, J.M., Denton, G.H., Barrell, D.J.A., Ivy-Ochs, S., Kubik, P.W., Andersen, B.G., Philips, F.M., Lowell, T.V., Schluchter, C., 2006. Near-synchronous interhemispheric termination of the last glacial maximum in mid-lattitudes. Science 312, 1510–1513.
Schouten, S., Huguet, C., Hopmans, E.C., Sinninghe Damsté, J.S., 2007. Improved analytical methodology of the TEX86 paleothermometry by high performance liquid chromatography/atmospheric pressure chemical ionization-mass spectrometry. Anal. Chem. 79, 2940–2944.
Sinninghe Damsté, J.S., Ossebaar, J., Schouten, S., Verschuren, S., 2008. Altitudinal shifts in the branched tetraether lipid distribution in soil from Mt. Kilimanjaro (Tanzania): implications for the MBT/CBT continental palaeothermometer. Org. Geochem. 39, 1072–1076.
Stevens, T., Thomas, D.S.G., Armitage, S.J., Lunn, H.R., Lu, H., 2007. Reinterpreting climate proxy records from late Quaternary Chinese loess: a detailed OSL investigation. Earth Sci. Rev. 80, 111–136.
Stuiver, M., Grootes, P.M., 2000. GISP2 oxygen isotope ratios. Quatern. Res. 53, 277–283.
Sun, J., Huang, X., 2006. Half-precessional cycles recorded in Chinese loess: response to low-latitude insolation forcing during the last glaciation. Quatern. Sci. Rev. 25, 1065–1072.
Sun, X., Song, C., Wang, F., Sun, M., 1997. Vegetation history of the loess plateau of china during the last 1000,000 years based on pollen data. Quatern. Int. 37, 25–36.
Tao, W., Huijun, W., Dabang, J., 2010. Mid-Holocene East Asian summer climate as simulated by the PMIP2 models. Palaeogeogr. Palaeoclimatol. Palaeoecol. 288, 93–102.
Tierney, J.E., Russell, J.M., Huang, Y., Sininghe Damsté, J.S., Hopmans, E.C., Cohen, A.S., 2008. Northern hemisphere controls on tropical southeast African climate during the past 60,000 years. Science 322, 252–255.
Wang, Y.J., Cheng, H., Edwards, R.L., An, Z.S., Wu, J.Y., Shen, C.-C., Dorale, J.A., 2001. A high-resolution absolute-dated late Pleistocene monsoon record from Hulu Cave, China. Science 294, 2345–2348.
Wang, Y., Cheng, H., Edwards, R.L., Kong, X., Shao, X., Chen, S., Wu, J., Jiang, X., Wang, X., An, Z., 2008. Millenial- and orbital-scale changes in the East Asian monsoon over the past 224,000 years. Nature 451, 1090–1093.
Weijers, J.W.H., Schouten, S., Spaargaren, O.C., Sinninghe Damsté, J.S., 2006. Occurrence and distribution of tetraether membrane in soils: implications for the use of the BIT index and the TEX_{86} SST proxy. Org. Geochem. 37, 1680–1693.
Weijers, J.W.H., Schefuß, E., Schouten, S., Sinninghe Damsté, J.S., 2007a. Coupled thermal and hydrological evolution of tropical Africa over the last deglaciation. Science 315, 1701–1704.
Weijers, J.W.H., Schouten, S., van den Donker, J.C., Hopmans, E.C., Sinninghe Damsté, J.S., 2007b. Environmental controls on bacterial tetraether membrane lipid distribution in soils. Geochim. Cosmochim. Acta 71, 703–713.
Weijers, J.W.H., Schouten, S., Sluijs, A., Brinkhuis, H., Sinninghe Damsté, J.S., 2007c. Warm arctic continents during the Palaeocene–Eocene thermal maximum. Earth Planet. Sc. Lett. 261, 230–238.
WMO, 2007. World Meteorological Organization. http://worldweather.wmo.int. On-line available.
Wu, N., Liu, T., Liu, X., Gu, Z., 2002. Mollusk record of millennial climate variability in the Loess Plateau during the Last Glacial Maximum. Boreas 31, 20–27.
Yuan, D., Cheng, H., Edwards, R.L., Dykoski, C.A., Kelly, M.J., Zhang, M., Qing, J., Lin, Y., Wang, Y., Wu, J., Dorale, J.A., An, Z., Cai, Y., 2004. Timing, duration and transitions of the last interglacial Asian monsoon. Science 304, 575–578.
Zheng, H., Huang, X., Ji, J., Liu, R., Zeng, Q., Jiang, F., 2007. Ultra-high rates of loess sedimentation at Zhengzhou since Stage 7: implication for the Yellow River erosion of the Sanmen Gorge. Geomorphology 85, 131–142.
Zhou, Z., Baoyin, Y., Petit-Maire, N., 1998. Paleoenvironments in China during the Last Glacial Maximum and the Holocene Optimum. Episodes 21, 152–158.